Science Bulletin 64 (2019) 478–484

Contents lists available at ScienceDirect

Science Bulletin

journal homepage: www.elsevier.com/locate/scib

Article

A dendrite-free Li plating host towards high utilization of Li metal anode in Li–O_2 battery

Chao Li, Jishi Wei, Panlong Li, Wenfei Tang, Wuliang Feng, Jingyuan Liu, Yonggang Wang *, Yongyao Xia

Department of Chemistry and Shanghai Key Laboratory of Molecular Catalysis and Innovative Materials, Institute of New Energy, iChEM (Collaborative Innovation Center of Chemistry for Energy Materials), Fudan University, Shanghai 200433, China

ARTICLE INFO

Article history:
Received 23 January 2019
Received in revised form 19 February 2019
Accepted 22 February 2019
Available online 6 March 2019

Keywords:
Li metal anode
Li utilization
Li–O_2 battery
Dendrite-free
High energy density

ABSTRACT

The intense interest of Li–O_2 battery stems from its ultrahigh theoretical energy density, but its application is still hindered by the issues of Li anode. Herein, RuO_2-CNTs composite, a conventional O_2 cathode catalyst in Li–O_2 battery, is first utilized as an anode host for dendrite-free Li plating/stripping with high Coulombic efficiency. It is demonstrated that such excellent plating/stripping performance arises from the lithiophilicity characteristic of Ru nanoparticles (that is derived from the in-situ electrochemical conversion from RuO_2 to Ru/Li_2O) and buffer space provided by CNTs. Furthermore, the RuO_2-CNTs electrode pre-deposited with limited Li (RuO_2-CNTs@Li anode) is coupled with a RuO_2-CNTs catalytic cathode to form a Li–O_2 full cell, which displays an extended cycle life with dramatically improved energy density. The achieved cell shows a high stability of 200 cycles with RuO_2-CNTs@Li anode (1 mg Li) that sheds light on the efficient utilization of Li anode in Li–O_2 batteries.

1. Introduction

Li–O_2 battery has received intense attention due to its super-high theoretical energy density [1–5]. In recent years, a lot of strategies, such as the catalysts design and electrolytes optimization, have been developed to improve the performance of O_2 cathode [6–13]. Nevertheless, the poor utilization efficiency of Li metal anode in Li–O_2 battery has never been improved. In most of previous reports [4–8,10–16], a much excess Li metal anode must be used to ensure the stable operation of Li–O_2 batteries, where the key reason is that the electrolyte containing O_2 and/or O_2^- can consume a lot of metallic Li (especially, these Li dendrites with high surface area) [17,18]. When calculated based on the total mass of catalyst in cathode and Li in anode, these reported Li–O_2 batteries generally exhibit very low energy densities, which are far away from the theoretical one or even lower than conventional Li-ion batteries.

In fact, the safe and efficient utilization of Li metal anode is a very old topic. During continuous plating/stripping, numerous Li dendrites formed on the surface of Li metal, which cause the safety issues. Simultaneously, the fresh formed Li dendrites react with electrolyte, which convert dendritic Li to electrochemically inert "dead" Li [19,20]. Recently, the investigation of Li metal anode was reemerged with extensive interest [21–34]. Various approaches, e.g., porous host materials coated with lithiophilic seeds [22,23], electrolyte optimization [24–26] and artificial solid electrolyte interphase (SEI) [27–31] were used to improve the behavior of Li plating/stripping. As a result, it has been demonstrated that several Li metal batteries (i.e. Li//$LiFePO_4$, Li//$Li_4Ti_5O_{12}$ and Li//$LiCoO_2$) can be stably cycled using a small amount of pre-deposited Li and the special electrolytes (e.g., LiTFSI dissolved in 1,3-dioxolane/1,2-dimethoxyethane (DOL/DME) with $LiNO_3$ additive or $LiPF_6$ dissolved in carbonate-based electrolyte) [20,23,30–34]. Unfortunately, these successful strategies have never been used in Li–O_2 batteries. One reason is that the presence of O_2 and O_2^- in Li–O_2 batteries intensely aggravates Li consumption, the other is that these optimized electrolytes for Li plating/stripping cannot be used to Li–O_2 batteries. Namely, it is still a huge challenge to increase the Li utilization in Li–O_2 batteries.

Herein, the RuO_2 nanoparticles anchored on carbon nanotubes (CNTs) was fabricated as RuO_2-CNTs composite, which is applied as a catalyst for O_2 cathode and the host for Li plating/stripping, showing double-function. It was found that the Ru nanoparticles (that is derived from the in-situ electrochemical conversion from RuO_2 to Ru/Li_2O) act as lithiophilic seeds to decrease the overpotential of Li nucleation and hysteresis during Li plating process, and the CNTs provide a buffer space to accommodate the deposited Li. After repeated Li plating/stripping processes in the electrolyte of 1 mol L^{-1} LiTFSI-DOL/DME with 2 wt% $LiNO_3$ additive, the RuO_2-

* Corresponding author.
E-mail address: ygwang@fudan.edu.cn (Y. Wang).

https://doi.org/10.1016/j.scib.2019.03.004
2095-9273/

CNTs@Li anode possesses Li dendrite-free morphology with a stable SEI layer that benefits the practical application. To serve as the anode of Li–O_2 battery, 5 mAh cm^{-2} (i.e. the 1 mg Li in considering the electrode area of 0.785 cm^2) Li was pre-deposited on RuO_2-CNTs electrode in 1 mol L^{-1} LiTFSI-DOL/DME electrolyte with 2 wt% $LiNO_3$ additive. The achieved RuO_2-CNTs@Li anode paired with RuO_2-CNTs cathode was then fabricated as a Li–O_2 full cell operated in 1 mol L^{-1} LiTFSI-tetraglyme (TEGDME) electrolyte. The corresponding Li–O_2 full cell reveals an extended cycle life with dramatically improved energy density, in comparison with that using a much excess Li anode.

2. Materials and methods

2.1. Material synthesis

50 mg CNTs were dispersed in a 0.01 mol L^{-1} $RuCl_3$ solution by ultrasonication for 10 min. A 0.03 mol L^{-1} $NaHCO_3$ solution was then slowly added to the above mixture under stirring until the pH value reached 7. After stirring for another 20 h, the precipitate was washed with distilled water and dried in air. The composite was then achieved by annealing in air at 150 °C for 19 h, which was donated as RuO_2-CNTs.

Ru-coated Cu (Cu@Ru) electrode was obtained by magnetron sputtering method. The ruthenium and Cu electrode serve as the sputtering target and the substrate, respectively. The mass loading of Ru on the Cu electrode was 0.4–0.5 mg after sputtering for 30 min.

2.2. Electrochemical measurements

The electrochemical test of Li plating/stripping process was measured in CR2016-type coin cells using 1 mol L^{-1} LiTFSI-DOL/DME (v:v = 1:1) electrolyte with 2 wt% $LiNO_3$ additive. 80 wt% RuO_2-CNTs (or CNTs, RuO_2 nanoparticles) and 20 wt% polyvinylidene fluoride binder (PVDF) were dissolved in N-methyl-2-polyvinylidene (NMP). The resulting slurry was then coated on Cu electrode and dried in a vacuum oven at 80 °C for 12 h. The obtained electrodes and commercial Li film were punched into disks with a diameter of 12 mm as the working electrode and counter electrode, respectively. To form a stable SEI layer and remove the surface contamination, the assembled cells were cycled between 0 and 2 V at 0.5 mA cm^{-2} for 20 cycles, previously. A fixed amount of Li was then plated onto prepared electrodes and stripped by charging to 2 V for each cycle.

2.3. Battery assembly

The RuO_2-CNTs@Li anode (i.e. the RuO_2-CNTs electrode was first cycled several times and then pre-deposited Li with 5 mAh cm^{-2} Li in 1 mol L^{-1} LiTFSI-DOL/DME electrolyte with 2 wt% $LiNO_3$ additive) was coupled with $LiFePO_4$ to form a full cell of Li//$LiFePO_4$. To prepare the $LiFePO_4$ electrode, the mixture slurry of $LiFePO_4$, super P, and PVDF in the mass ratio of 8:1:1 was dispersed in NMP and then coated onto Al foil. The mass loading of $LiFePO_4$ is about 4 mg cm^{-2}. The Li//$LiFePO_4$ cells were tested between 2 and 4.3 V using 1 mol L^{-1} LiTFSI-DOL/DME electrolyte with 2 wt% $LiNO_3$ additive.

To prepare RuO_2-CNTs cathode, the slurry of 80 wt% RuO_2-CNTs and 20 wt% PVDF was mixed in NMP, and then pasted on a carbon paper. The mass loading of RuO_2-CNTs in cathode is 0.5–0.6 mg cm^{-2}. To prepare the RuO_2-CNTs@Li anode, the RuO_2-CNTs electrode was firstly cycled several times in the electrolyte of 1 mol L^{-1} LiTFSI-DOL/DME with 2 wt% $LiNO_3$ additive, and then pre-deposited with 5 mAh cm^{-2} Li (1 mg Li in considering the electrode area of 0.785 cm^2). Prior to the Li–O_2 full cell assembly, the prepared RuO_2-CNTs@Li anode was washed with TEGDME solvent. The RuO_2-CNTs cathode and RuO_2-CNTs@Li anode (or commercial Li film) were separated by a separator (commercial celegard membrane) dipping with 1 mol L^{-1} LiTFSI-TEGDME electrolyte. The electrolyte volume was ~50 μL for each Li–O_2 battery. Such anode/separator/cathode was then sealed into a home-made Li–O_2 cell, which possesses a hole with a diameter of 1 cm (~ 0.785 cm^2) to guarantee the O_2 flowing in cathode side. The electrochemical measurements of Li–O_2 cells were employed by Land cycler (Wuhan Land Electronic Co. Ltd) in a pure/dry oxygen-filled glove box. The capacities and current densities are calculated based on the mass loading of RuO_2-CNTs in cathode. The energy density of Li–O_2 cell is calculated based on the total mass of catalyst in cathode and Li in anode.

2.4. Material characterization

The mass ratio of RuO_2 in RuO_2-CNTs composite was measured with a TG209F1 thermo-gravimetric (TG) analysis instrument (NETZSCH) under O_2 (heating rate of 10 °C min^{-1}). X-ray diffraction (XRD) measurements of RuO_2-CNTs and CNTs were carried out on a Bruker D8 Focus power X-ray diffractometer with Cu Kα radiation. The Raman spectra were performed to characterize RuO_2-CNTs and CNTs on Reni Shaw inVia Laser Scanning Confocal Microscopy (excitation wavelength: 632.8 nm). X-ray photoelectron spectroscopy (XPS) was carried out to detect the SEI layer on the surface of RuO_2-CNTs electrode using a XSAM800 Ultra spectrometer. Fourier transform infrared spectroscopy (FT-IR) data were achieved on a Nicolet 6700 spectrometer. The morphology of RuO_2-CNTs was observed by scanning electron microscopy (SEM) on a Hitachi S-4800 microscope and transmission electron microscopy (TEM) on a FEI Tecnai G20 field emission electron microscope operated at 200 kV. Elemental mapping of RuO_2-CNTs was collected by energy-dispersive spectrometer (EDS) mapping equipped on TEM. The morphologies of RuO_2-CNTs, CNTs, RuO_2 and Cu electrode at pristine stage and after Li plating with 2 mAh cm^{-2} were analyzed by SEM. To observe the morphology of plated Li, the discharged electrodes were obtained by disassembling the cells in an Ar-filled glove box. The RuO_2-CNTs@Li, CNTs@Li, RuO_2@-Li, and Cu@Li electrodes were washed by DME solvent to remove LiTFSI salt and residual electrolyte before SEM characterization. The morphologies of RuO_2-CNTs@Li anode (5 mAh cm^{-2} pre-deposited Li) and commercial Li film anode used in Li–O_2 cells were also characterized by SEM at pristine stage and after 60th cycle, respectively. The RuO_2-CNTs cathodes with different discharge/charge stages in Li–O_2 full cells were examined by ex situ SEM, XRD and FT-IR, respectively.

3. Results and discussion

The RuO_2-CNTs composite is obtained by a mild sol-gel method. The 3D network structure of CNTs precursor is characterized by SEM images (Fig. S1a and S1b online). The SEM image of the RuO_2-CNTs composite is given in Fig. 1a, showing that the 3D structure of the sample is well maintained after the decoration of RuO_2 nanoparticles. The high-resolution TEM image (Fig. 1b) of the sample indicates that the typical diameter of these RuO_2 nanoparticles is ~2 nm. The TEM image (Fig. 1c) and corresponding EDS mapping of elements C, Ru, and O (Fig. 1d–f) further confirm the decoration of RuO_2 on CNTs. The XRD patterns of the RuO_2-CNTs composite and CNTs are given in Fig. 1g, where it can be observed that the diffraction peaks of CNTs are decreased with the decorating of RuO_2. The diffraction peaks (red lines of Fig. 1g) located around 28°, 35°, 40° and 54° can be indexed to RuO_2

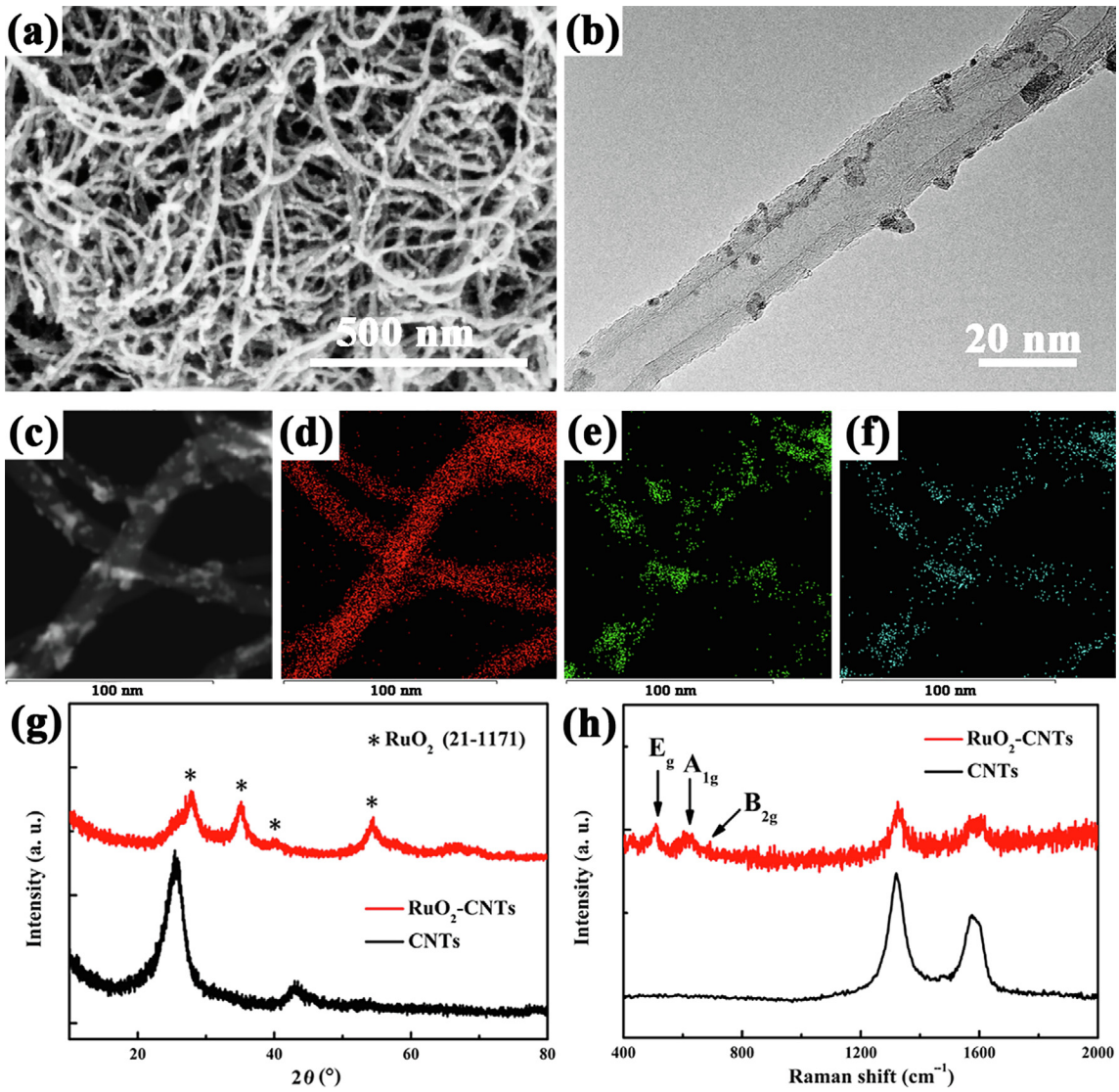

Fig. 1. Characterizations of RuO_2-CNTs composite. (a) SEM and (b) TEM image of RuO_2-CNTs. (c) TEM image of RuO_2-CNTs and (d)–(f) the corresponding EDS mapping images of C, Ru and O elements. (g) XRD pattern and (h) Raman spectra of RuO_2-CNTs and CNTs, respectively.

(PDF No. 43-1027). The Raman spectra of RuO_2-CNTs composite and CNTs (Fig. 1h) indicates that both samples display a D-band (around 1,320 cm^{-1}) and a G-band (around 1,580 cm^{-1}), corresponding to the carbonaceous material [35]. However, the peak intensity of RuO_2-CNTs composite is much weaker than that of CNTs. The new peaks located at around 515 (E_g), 630 (A_{1g}), and 691 (B_{2g}) cm^{-1} in the Raman spectra can be attributable to the three Raman active modes of RuO_2 [35]. The mass ratio of RuO_2 nanoparticles (~50 wt%) in the composite is confirmed by thermogravimetric (TG) analysis (Fig. S2 online).

The catalytic activity of RuO_2-CNTs composite in Li–O_2 battery has been demonstrated in Zhou et al.'s previous report [35]. Herein we focus on the Li plating/stripping performance of the RuO_2-CNTs composite, which was investigated in 1 mol L^{-1} LiTFSI-DOL/DME electrolyte with 2 wt% $LiNO_3$ additive. For comparison, the Li plating/stripping profiles of bare CNTs, RuO_2 nanoparticles (Fig. S3 online) and conventional Cu electrode were also investigated at the same condition. Fig. 2a presents the comparison of Coulombic efficiency using RuO_2-CNTs, CNTs, RuO_2 and Cu electrodes with a plating capacity of 2 mAh cm^{-2} at a current density of 1 mA cm^{-2}. As shown in Fig. 2a, the RuO_2-CNTs electrode reveals a stable Coulombic efficiency with a long-term running that is superior to other electrodes. The corresponding discharge/charge profiles of RuO_2-CNTs electrode at different cycles are shown in Fig. S4 (online). The differences of these electrodes are further clarified by the comparison of the discharge/charge curves at selected cycles (1st, 70th and 135th cycles). As shown in Fig. 2b, these electrodes exhibit the initial Coulombic efficiencies of 94.8% (RuO_2-CNTs electrode), 93.6% (CNTs electrode), 91.0% (RuO_2 electrode) and 85.7% (Cu electrode), respectively. Furthermore, the hysteresis of Cu electrode at 1st cycle is much larger than that of other electrodes (inset of Fig. 2b). The Coulombic efficiency of Cu electrode (87.3%) is still much lower than that of other electrodes (>97%) with a large hysteresis at 70th cycle (Fig. 2c and inset), reflecting the instability of Cu electrode in Li plating/stripping process. At 135th cycle, both CNTs and RuO_2 electrodes deliver slumped Coulombic efficiencies (below 85%) and increased hysteresis, which is far inferior to that of RuO_2-CNTs electrode (Fig. 2d and inset). When conducted with larger plating capacities (5 and 10 mAh cm^{-2}), the RuO_2-CNTs electrode still maintains an eminent Coulombic efficiencies with long lifespans (Fig. S5 online). In a addtion, the corresponding

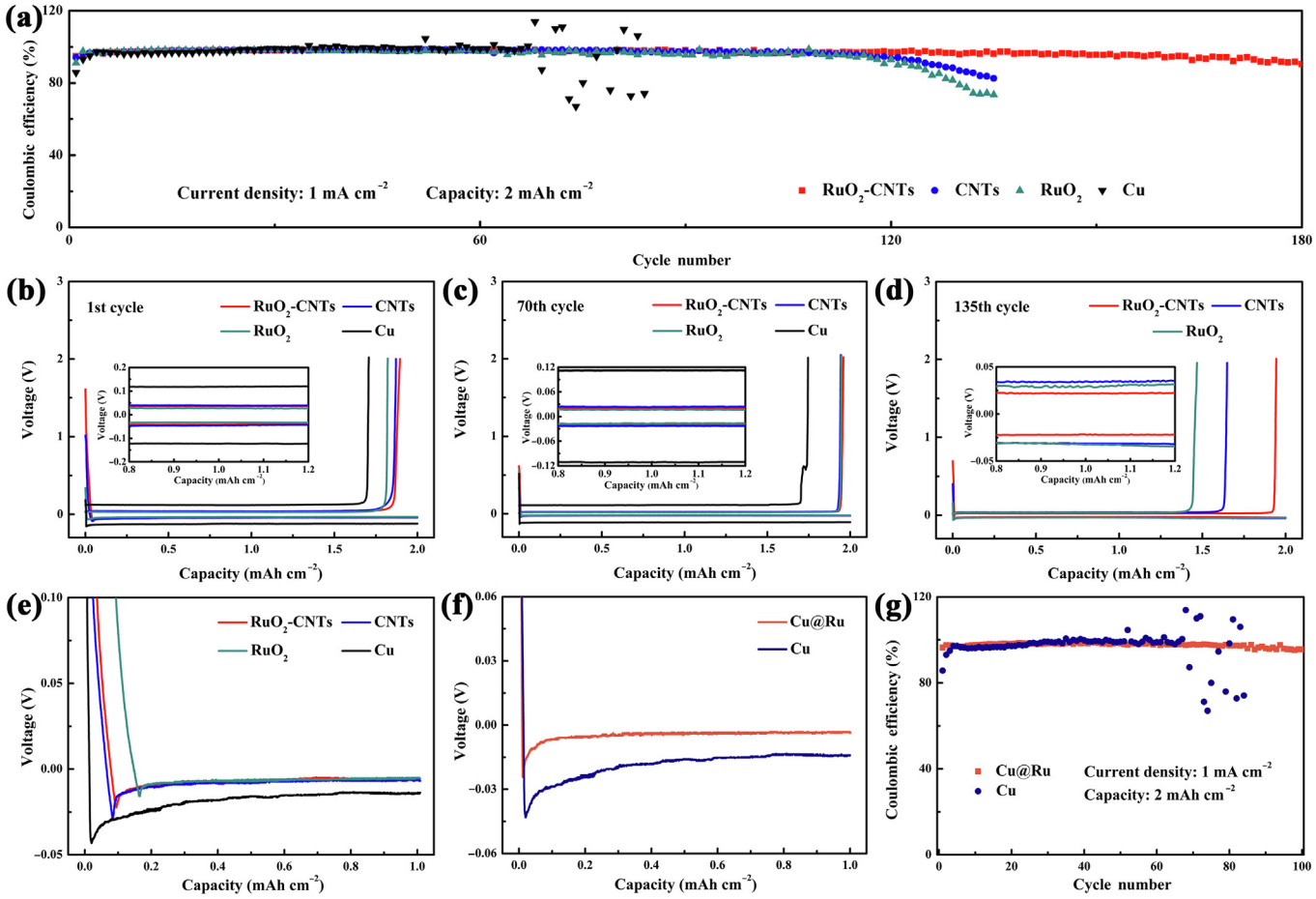

Fig. 2. Li plating/stripping performance of the RuO_2-CNTs host. (a) Comparison of Coulombic efficiency using RuO_2-CNTs, CNTs, RuO_2 and Cu electrode, respectively. Discharge/charge voltage profiles of Li plating/stripping process with various electrodes on (b) 1st cycle, (c) 70th cycle and (d) 135th cycle. Insets in (b)–(d) are the enlargements of hysteresis in the corresponding voltage profiles. (e) The voltage curves of Li nucleation using various electrodes at 0.05 mA cm^{-2}. (f) The voltage curves of Li nucleation using Cu@Ru and Cu electrodes at 0.05 mA cm^{-2}, respectively. (g) Comparison of Coulombic efficiency using Cu@Ru and Cu electrodes, respectively.

cycling performance might be improved by using artificial SEI layer to protect the electrode in further studies.

In order to compare the lithiophilicity of these electrodes, the nucleation overpotentials were measured at a low current density of 0. 05 mA cm^{-2} (Fig. 2e). The measurements and calculation of Li nucleation overpotential are according to the previous reports [22]. As shown in Fig. 2e, the RuO_2 electrode delivers the smallest voltage dip at the nucleation stage, showing a lowest nucleation overpotential. The nucleation overpotential of RuO_2-CNTs electrode is slightly higher than that of RuO_2 electrode, but is lower than that of CNTs and Cu electrodes. This result demonstrates that the RuO_2 benefits the Li nucleation. It is well known that the discharge/charge of RuO_2 nanoparticles should experience the reversible conversion reaction between RuO_2 and Ru/Li_2O [36–38], which is demonstrated by Fig. S6 (online). Therefore, the lithiophilicity of RuO_2-CNTs or RuO_2 electrode may arise from the existence of Ru on Li plating process. To clarify the lithiophilicity of Ru element, we prepared Ru-coated Cu electrode (i.e. Cu@Ru electrode) by using magnetron sputtering method. The Ru nanoparticles are uniformly deposited on the surface of Cu electrode (Fig. S7 online). The voltage curves of Li nucleation using Cu@Ru and Cu electrodes are performed at 0.05 mA cm^{-2} (Fig. 2f). The curve of Cu@Ru electrode shows a reduced voltage dip at the stage of Li nucleation and a lower nucleation overpotential (20.5 mV), which is evidently superior to that of Cu electrode (29.1 mV). This result indicates the lithiophilicity characteristic of Ru, which is beneficial to the Li plating/stripping behavior of RuO_2-CNTs electrode. The Cu@Ru electrode also exhibits a high Coulombic efficiency (96.5%) and long life for Li plating/stripping, which far exceeds that of the Cu electrodes (Fig. 2g), revealing that the surface of Ru-based electrode is more favorable for Li plating/stripping process with an eminent behavior. Although Li plating/stripping performance of Cu@Ru electrode is outstanding (100 cycles), it is still inferior to that of RuO_2-CNTs electrode (180 cycles). This result can be ascribed to the absence of 3D host structure that might cause the volume expansion of Cu@Ru electrode during cycling.

After electrochemical investigation, the SEM characterization was carried out to probe the Li dendrites formation of these electrode after Li plating. Fig. 3a–d present the SEM images of pristine RuO_2-CNTs electrode, CNTs electrode, RuO_2 electrode and Cu electrode. The corresponding SEM images of various electrodes after Li plating (2 mAh cm^{-2}) are shown in Fig. 3e–h. After plating (2 mAh cm^{-2}), the morphology of RuO_2-CNTs@Li electrode presents a smooth and uniform surface without dendritic Li (Fig. 3e), which should be attributable to the combination of lithiophilicity characteristic of Ru nanoparticles (through the in-situ electrochemical conversion from RuO_2 to Ru/Li_2O) and the 3D host structure of CNTs. On the contrary, the dendritic growth of Li emerges after Li plating on CNTs electrode (Fig. 3f), which is derived from the lack of the lithiophilic seeds for Li deposition. The Li dendrites also appear on RuO_2 electrode (Fig. 3g) after Li plating because of the absence of 3D buffer. When switching to

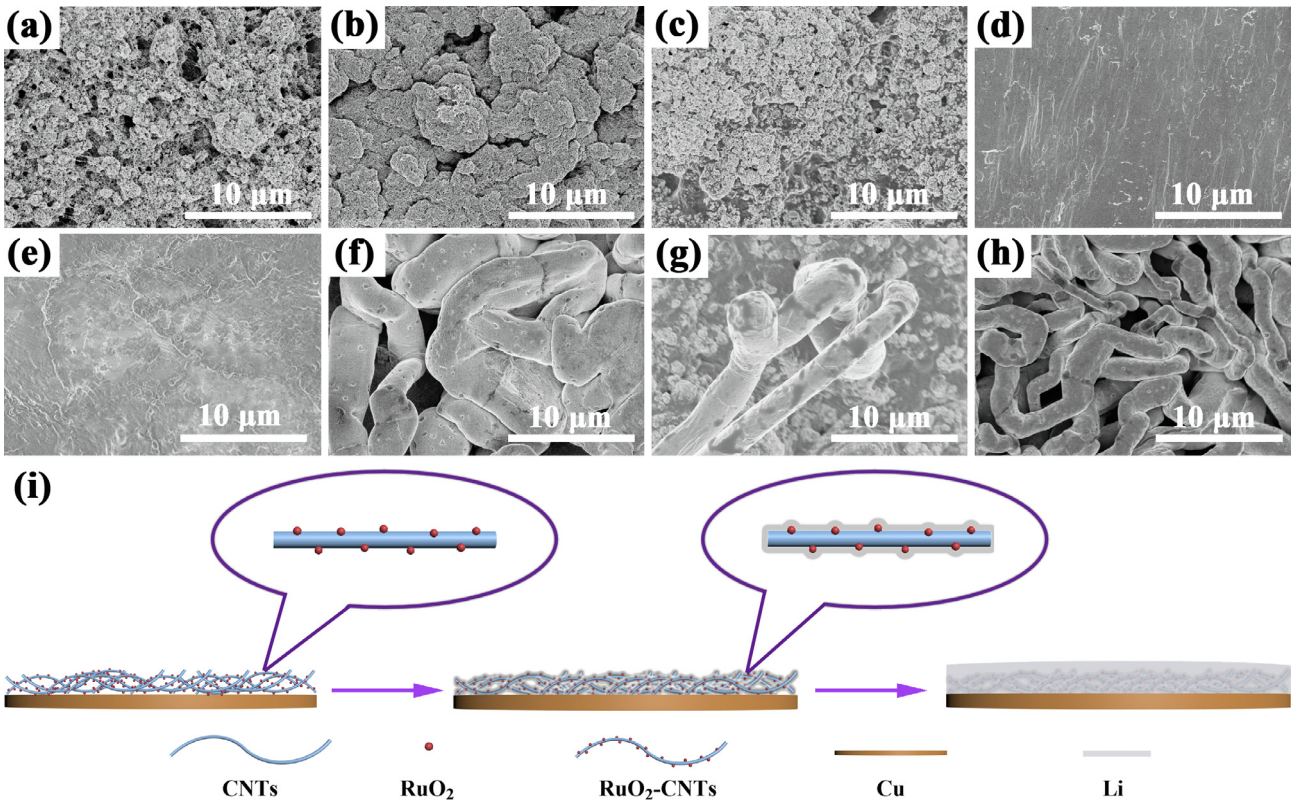

Fig. 3. SEM characterization of various electrodes. SEM images of pristine (a) RuO_2-CNTs electrode, (b) CNTs electrode, (c) RuO_2 electrode and (d) Cu electrode. The morphologies of (e) RuO_2-CNTs electrode, (f) CNTs electrode, (g) RuO_2 electrode and (h) Cu electrode after Li plating with the capacity of 2 mAh cm^{-2} at the current density of 1 mA cm^{-2}, respectively. (i) Schematic diagram of Li uncleation and deposition on RuO_2-CNTs electrode.

the Cu electrode, numerous Li dendrites with a mean diameter of ~1 μm (Fig. 3h) are deposited on Cu electrode. Furthermore, the cross-section SEM images also confirm the smooth and uniform surface of RuO_2-CNTs@Li electrode (Fig. S8 online). The data shown in Fig. 3a–h indicate that the unique structure of RuO_2-CNTs can efficiently prevent the dendrites formation, which is illustrated by Fig. 3i. As shown in Fig. 3i, the RuO_2 nanoparticles offer numerous lithiophilic sites to induce the Li deposition with a lower nucleation overpotential, and the 3D network structure supplies the sufficient buffer for deposited Li. Accordingly, the Li nucleates preferentially on the surface of RuO_2, and then generates a uniform and smooth morphology on RuO_2-CNTs electrode after the Li plating.

To further demonstrate the promising performance RuO_2-CNTs electrode in practical cell, the RuO_2-CNTs@Li electrode (i.e. the RuO_2-CNTs electrode pre-deposited with 5 mAh cm^{-2} Li) was coupled with $LiFePO_4$ to form a full cell of Li//$LiFePO_4$ using the electrolyte of 1 mol L^{-1} LiTFSI in DOL/DME with 2 wt% $LiNO_3$ additive, which is similar to previous reports [21,23,30,32,34]. Fig. S9 (online) shows an outstanding cycling stability for 500 cycles with a capacity retention of ~75%, which is superior to most previous reports (See Table S1 online for more details). As mentioned at beginning, the key purpose of present work is to increase the utilization of Li in Li–O_2 battery. Therefore, the RuO_2-CNTs@Li electrode was then used to build a Li–O_2 battery. In this experiment, the RuO_2-CNTs electrode was firstly cycled several times in the electrolyte of 1 mol L^{-1} LiTFSI in DOL/DME with 2 wt% $LiNO_3$ additive, and then pre-deposited with 5 mAh cm^{-2} Li (i.e. the 1 mg Li in considering the electrode area of 0.785 cm^2) to form the RuO_2-CNTs@Li electrode. We note that the Li–O_2 battery is inadaptable to operate in the electrolyte that utilized in Li plating/stripping test (Fig. S10 online), while the Li plating/stripping behavior of RuO_2-CNTs electrode is far from satisfactory in the electrolyte of 1 mol L^{-1} LiTFSI-TEGDME (Fig. S11 online). Hence, different electrolytes should be employed for the preparation of RuO_2-CNTs@Li anode and operation of Li–O_2 full cell, respectively. The prepared RuO_2-CNTs@Li electrode is coated with a solid electrolyte interphase (SEI) film, which is confirmed by XPS and FT-IR characterization (Fig. S12 online). Such SEI film may prevent the O_2 attacking on anode, which can be further clarified by Li–O_2 full cell tests. A Li–O_2 full cell was assembled by using a RuO_2-CNTs based catalytic electrode as cathode and a RuO_2-CNTs@Li as anode in the electrolyte of 1 mol L^{-1} LiTFSI-TEGDME. In this cell, the RuO_2-CNTs shows the double-function (i.e. the catalyst for O_2 and the host for Li plating/stripping). A conventional Li–O_2 full cell with a much excess Li film anode (Fig. S13 online) was fabricated at the same condition for comparison. As shown in Fig. S13, the thickness of the Li film (40 mg per 0.785 cm^2) is about 972 μm, which is widely used for Li–O_2 battery investigation [11,13–15,18]. Fig. 4a presents the full discharge curves of both cells at a current density of 100 mA g^{-1}, where the current density is calculated only based on the mass of RuO_2-CNTs in cathode (such method is widely used in previous reports [4,6,8–18,35]). The achieved full discharge capacity (3,776 mAh g^{-1}) of the cell using RuO_2-CNTs@Li anode is just slightly higher than that (3,545 mAh g^{-1}) of the cell using commercial Li film anode. However, when calculated based on total mass of catalyst in cathode and Li in anode, the cell using RuO_2-CNTs@Li anode exhibits much higher energy density (2,850 Wh kg^{-1}) than that (93 Wh kg^{-1}) of the cell using commercial Li film anode (Fig. 4b). Cycle performance of the both cells was tested with a fixed capacity of 500 mAh g^{-1} at a current density of 250 mA g^{-1}. As shown in Fig. 4c, the Li–O_2 full cell using RuO_2-CNTs@Li anode delivers a remarkable cycle life. The load curves are stable over 200 cycles without capacity fade. As a contrast, the rechargeability of Li–O_2

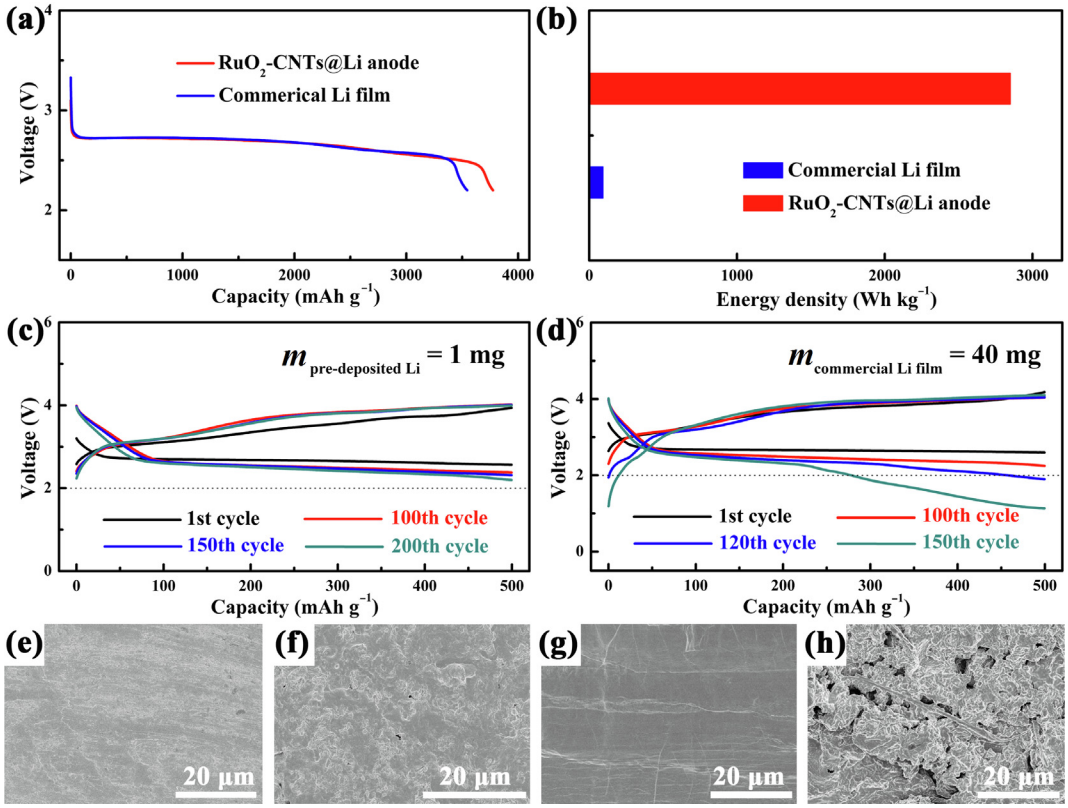

Fig. 4. Electeochemical performacne of Li–O_2 battery. (a) The discharge profiles of RuO_2-CNTs based Li–O_2 cells at 100 mA g^{-1} with different anodes and (b) corresponding energy densities. Recyclability of Li–O_2 batteries with a fixed capacity 500 mAh g^{-1} at 250 mA g^{-1} using (c) RuO_2-CNTs@Li anode and (d) commercial Li film anode. SEM images of RuO_2-CNTs@Li anode (e) at pristine stage and (f) after 60th cycle. (g) and (h) SEM are images of commercial Li film anode at pristine stage and after 60th cycle, respectively.

battery with commercial Li film anode is inferior to that using RuO_2-CNTs@Li anode (Fig. 4d). The terminal discharge voltage degrades to <2.0 V at 120th cycle. The energy density (calculated based on the total mass of catalyst in cathode and Li in anode) of the Li–O_2 full cell using RuO_2-CNTs@Li anode reaches ~400 Wh kg^{-1}. It should be noted that the RuO_2-CNTs@Li anode still possesses excess Li, which guarantees the operation of Li–O_2 battery with higher discharge/discharge depth. When increased the fixed capacity to 1,000 mAh g^{-1}, the cell using RuO_2-CNTs@Li anode exhibits a high energy density of approximately 766 Wh kg^{-1} with a promising cycling stability over initial 60 cycles (Fig. S14 online). Nevertheless, when the Li amount on RuO_2-CNTs@Li anode is reduced, the cycling stability of corresponding Li–O_2 full cell delivers sharp decline (Fig. S15 online). The reversibility of cathode in the cell was investigated by using ex situ SEM, XRD and FT-IR, indicating that Li_2O_2 serves as the dominant discharge product and disappears after recharge reversibly (Fig. S16 online). Fig. 4e and g present the SEM images of the pristine RuO_2-CNTs@Li anode and commercial Li film anode for Li–O_2 batteries. The corresponding SEM images of these electrodes after Li plating (i.e. recharged Li–O_2 batteries after 60th cycle) are shown in Figs. 4f and h, respectively. It can be observed that the cycled RuO_2-CNTs@Li anode still maintains an even morphology without dendritic Li (Fig. 4f), whereas the cycled Li film anode presents cracks and Li dendrites (Fig. 4h). Such dendrite-free anodes might impel the long time running of related Li–O_2 battery. It is worth noting that the consumption of Li in anode is inevitable due to the decomposition of ethers-based electrolytes, irreversible byproducts and the corrosion of dissolved O_2. In general, a much excess amount of Li, such as commercial Li film, is utilized to guarantee a long lifespan operation of Li anode, which greatly decreases the energy density of Li–O_2 batteries. To manifest the significance of RuO_2-CNTs@Li anode in Li–O_2 battery, we compare the usage rate of Li amount in anode. As shown in Table S2 (online), the utilization of RuO_2-CNTs@Li anode realizes a much higher usage rate of Li with an extremely improved energy density, which far exceed that using commercial Li film or Li foil in most prior works. Increasing the utilization of Li pioneers a new avenue of designing high-efficiency anode towards real Li–O_2 electrochemistry.

4. Conclusion

In summary, the safe and efficient utilization of Li anode is an old issue, which must urgently be addressed in Li–O_2 batteries. The much excess Li anode and the dendrites formation limit the practical energy density and safety operation of most Li–O_2 batteries. In this work, it has been demonstrated that the RuO_2-CNTs electrode realizes the uniform Li deposition without Li dendrites, which arises from the lithiophilicity characteristic of Ru nanoparticles (through the in-situ electrochemical conversion from RuO_2 to Ru/Li_2O) and the 3D host structure of CNTs. Furthermore, it is found that the RuO_2-CNTs@Li electrode coated with SEI film can ensure the stable operation of Li–O_2 batteries with very limited Li in anode, through which Li–O_2 batteries can achieve higher energy density and better cycle life.

Conflict of interest

The authors declare that they have no conflict of interest.

Acknowledgments

This work was supported by the National Natural Science Foundation of China (21622303) and the National Basic Research Program of China (2016YFA0203302).

Author contributions

C. Li and Y. Wang conceived the idea and co-wrote the manuscript. C. Li designed and performed the experiments. J. Wei, P. Li, W. Tang, W. Feng and J. Liu assisted with the material characterizations and data analysis. All authors contributed to the discussion. Y. Wang and Y. Xia supervised the project.

Appendix A. Supplementary data

Supplementary data to this article can be found online at https://doi.org/10.1016/j.scib.2019.03.004.

References

[1] Aurbach D, Mccloskey BD, Nazar LF, et al. Advances in understanding mechanisms underpinning lithium–air batteries. Nat Energy 2016;1:16128.
[2] Geng D, Ding N, Andy Hor TS, et al. From lithium-oxygen to lithium-air batteries: challenges and opportunities. Adv Energy Mater 2016;6:1502164.
[3] Feng N, He P, Zhou H. Critical challenges in rechargeable aprotic Li–O_2 batteries. Adv Energy Mater 2016;6:1502303.
[4] Lu J, Lee YJ, Luo X, et al. A lithium–oxygen battery based on lithium superoxide. Nature 2016;529:377–82.
[5] Guo X, Sun B, Su D, et al. Recent developments of aprotic lithium-oxygen batteries: functional materials determine the electrochemical performance. Sci Bull 2017;62:442–52.
[6] Xu SM, Liang X, Ren ZC, et al. Free-standing air cathodes based on 3D hierarchically porous carbon membranes: kinetic overpotential of continuous macropores in Li–O_2 batteries. Angew Chem Int Ed 2018;57:6825–9.
[7] Yang ZD, Chang ZW, Zhang Q, et al. Decorating carbon nanofibers with Mo_2C nanoparticles towards hierarchically porous and highly catalytic cathode for high-performance Li–O_2 batteries. Sci Bull 2018;63:433–40.
[8] Jung HG, Hassoun J, Park JB, et al. An improved high-performance lithium-air battery. Nat Chem 2012;4:579–85.
[9] Liu T, Frith JT, Kim G, et al. The effect of water on quinone redox mediators in nonaqueous Li–O_2 batteries. J Am Chem Soc 2018;140:1428–37.
[10] Zhang Y, Wang L, Zhang X, et al. High-capacity and high-rate discharging of a coenzyme Q_{10}-catalyzed Li–O_2 battery. Adv Mater 2017;30:1705571.
[11] Zhang J, Sun B, Zhao Y, et al. Modified tetrathiafulvalene as an organic conductor for improving performances of Li–O_2 batteries. Angew Chem Int Ed 2017;56:8505–9.
[12] Giordani V, Tozier D, Tan H, et al. A molten salt lithium-oxygen battery. J Am Chem Soc 2016;138:2656–63.
[13] Guo Z, Li C, Liu J, et al. A long-life lithium-air battery in ambient air with a polymer electrolyte containing a redox mediator. Angew Chem Int Ed 2017;56:7505–9.
[14] Zhu J, Yang J, Zhou J, et al. A stable organic-inorganic hybrid layer protected lithium metal anode for long-cycle lithium-oxygen batteries. J Power Sources 2017;366:265–9.
[15] Kim Y, Koo D, Ha S, et al. Two-dimensional phosphorene-derived protective layers on a lithium metal anode for lithium-oxygen batteries. ACS Nano 2018;12:4419–14330.
[16] Zhang X, Zhang Q, Wang XG, et al. An extremely simple method for protecting lithium anodes in Li–O_2 batteries. Angew Chem Int Ed 2018;57:12814–8.
[17] Wu S, Zhu K, Tang J, et al. A long-life lithium ion oxygen battery based on commercial silicon particles as the anode. Energy Environ Sci 2016;9:3262–71.
[18] Xu JJ, Liu QC, Yu Y, et al. In Situ Construction of stable tissue-directed/reinforced bifunctional separator/protection film on lithium anode for lithium-oxygen batteries. Adv Mater 2017;29:1606552.
[19] Lin D, Liu Y, Cui Y. Reviving the lithium metal anode for high-energy batteries. Nat NanoTechnol 2017;12:194–206.
[20] Guo Y, Li H, Zhai T. Reviving lithium-metal anodes for next-generation high-energy batteries. Adv Mater 2017;29:1700007.
[21] Liu S, Wang A, Li Q, et al. Crumpled graphene balls stabilized dendrite-free lithium metal anodes. Joule 2018;2:184–93.
[22] Zhang R, Chen XR, Chen X, et al. Lithiophilic sites in doped graphene guide uniform lithium nucleation for dendrite-free lithium metal anodes. Angew Chem Int Ed 2017;56:7764–8.
[23] Liu L, Yin YX, Li JY, et al. Uniform lithium nucleation/growth induced by lightweight nitrogen-doped graphitic carbon foams for high-performance lithium metal anodes. Adv Mater 2018;30:1706216.
[24] Fan L, Wei S, Li S, et al. Recent progress of the solid-state electrolytes for high-energy metal-based batteries. Adv Energy Mater 2018;8:1702657.
[25] Qian J, Henderson WA, Xu W, et al. High rate and stable cycling of lithium metal anode. Nat Commun 2015;6:6362.
[26] Han X, Gong Y, Fu K, et al. Negating interfacial impedance in garnet-based solid-state Li metal batteries. Nat Mater 2017;16:572–9.
[27] Gu Y, Wang WW, Li YJ, et al. Designable ultra-smooth ultra-thin solid-electrolyte interphases of three alkali metal anodes. Nat Commun 2018;9:1339.
[28] Fan X, Chen L, Ji X, et al. Highly fluorinated interphases enable high-voltage Li-metal batteries. Chem 2018;4:174–85.
[29] Xie J, Liao L, Gong Y, et al. Stitching h-BN by atomic layer deposition of LiF as a stable interface for lithium metal anode. Sci Adv 2017;3:eaao3170.
[30] Assegie AA, Cheng JH, Kuo LM, et al. Polyethylene oxide film coating enhances lithium cycling efficiency of an anode-free lithium-metal battery. Nanoscale 2018;10:6125–38.
[31] Yan C, Yao YX, Chen X, et al. Solvation chemistry of lithium nitrate in carbonate electrolyte for high-voltage lithium metal battery. Angew Chem Int Ed 2018;57:14055–9.
[32] Zuo TT, Wu XW, Yang CP, et al. Graphitized carbon fibers as multifunctional 3D current collectors for high areal capacity Li anodes. Adv Mater 2017;29:1700389.
[33] Zhang C, Lv W, Zhou G, et al. Prestoring lithium into stable 3D nickel foam host as dendrite-free lithium metal anode. Adv Energy Mater 2018;8:1703404.
[34] Jin C, Sheng O, Luo J, et al. 3D lithium metal embedded within lithiophilic porous matrix for stable lithium metal batteries. Nano Energy 2017;37:177–86.
[35] Jian Z, Liu P, Li F, et al. Core-shell-structured CNT@RuO_2 composite as a high-performance cathode catalyst for rechargeable Li–O_2 batteries. Angew Chem Int Ed 2014;53:442–6.
[36] Gregorczyk KE, Kozen AC, Chen X, et al. Fabrication of 3D core-shell multiwalled carbon nanotube@RuO_2 lithium-ion battery electrodes through a RuO_2 atomic layer deposition process. ACS Nano 2015;9:464–73.
[37] Balaya BP, Li H, Kienle L, et al. Reversible homogeneous and heterogeneous Li storage in RuO_2 with high capacity. Adv Func Mater 2003;13:621–5.
[38] Delmer BO, Balaya P, Kienle L, et al. Enhanced potential of amorphous electrode materials: case study of RuO_2. Adv Mater 2008;20:501–5.

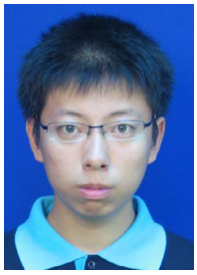

Chao Li received his B.S. degree in Chemistry from Fudan University in 2015. He is currently a Ph.D. candidate in Physical Chemistry from Fudan University. His research focuses on Li-air battery, Li metal anode and Li-CO_2 battery.

Yonggang Wang received his Ph.D. degree in Physical Chemistry from Fudan University in 2007. From 2007 to 2011, he worked as a Post-doctoral Research Associate at the National Institute of Advanced Industrial Science and Technology (AIST), Japan. He is currently a full professor at the Department of Chemistry at Fudan University, China. His research interests include energy storage/conversion devices, supercapacitor, Li-sulfur batteries, Li-air batteries, wearable and flexible energy storage devices.